A versatile high-throughput assay based on 3D ring-shaped cardiac tissues generated from human induced pluripotent stem cell derived cardiomyocytes

Magali Seguret[1], **Patricia Davidson**[2], **Stijn Robben**[2], **Charlène Jouve**[1], **Céline Pereira**[1], **Cyril Cerveau**[2], **Maël Le Berre**[2], **Rita S. Rodrigues Ribeiro**[2*], **Jean-Sébastien Hulot**[1*]

***For correspondence:** jean-sebastien.hulot@inserm.fr (FMS); ana-rita.ribeiro@4dcell.com (FS)

Present address: [§]Paris Cardiovascular Research Center, 56 Rue Leblanc, Paris, France

[1]Université de Paris Cité, PARCC, INSERM, F-75015 Paris, France; [2]4DCell, Montreuil, France

Abstract We developed a 96-well plate assay which allows fast, reproducible and high-throughput generation of 3D cardiac rings around a deformable optically transparent hydrogel (PEG) pillar of known stiffness. Human induced pluripotent stem cell-derived cardiomyocytes, mixed with normal human adult dermal fibroblasts in an optimized 3:1 ratio, self-organized to form ring-shaped cardiac constructs. Immunostaining showed that the fibroblasts form a basal layer in contact with the glass, stabilizing the muscular fiber above. Tissues started contracting around the pillar at D1 and their fractional shortening increased until D7, reaching a plateau at 25±1%, that was maintained up to 14 days. The average stress, calculated from the compaction of the central pillar during contractions, was 1.4±0.4 mN/mm2. The cardiac constructs recapitulated expected inotropic responses to calcium and various drugs (isoproterenol, verapamil) as well as the arrhythmogenic effects of dofetilide. This versatile high-throughput assay allows multiple in situ mechanical and structural read-outs.

Introduction

Cardiac tissue engineering (CTE) aims to generate *in vitro* cell constructs that recapitulate the intricate structural and functional properties of the native myocardium (***van der Velden et al., 2022***). As the heart lacks regenerative capacities, CTE emerged in the field of regenerative medicine with the objective of producing cardiac grafts that can be implanted in patients with heart failure (***Madonna et al., 2019***; ***Jabbour et al., 2021***; ***Eschenhagen et al., 2022***). In parallel, the rapid development of biomaterials and microfabrication techniques, combined with progress in pluripotent stem cell biology have enabled the generation of miniature engineered heart tissues (EHTs) used as "hearts-on-chips" or cardiac organoids models. While these EHTs recapitulate a limited number of functions *in vitro*, they have provided essential platforms for cardiac disease modeling (***Filippo Buono et al.*** (***2020***); ***Cashman et al.*** (***2016***); ***Williams et al.*** (***2021***); ***Stillitano et al.*** (***2016***); ***Bliley et al.*** (***2021***); ***Goldfracht et al.*** (***2019***); ***Richards et al.*** (***2020***)) and drug development (***Beauchamp et al.*** (***2015***); ***Polonchuk et al.*** (***2017***); ***Zhao et al.*** (***2019***); ***Mannhardt et al.*** (***2020***)), reducing the need for animal studies.

Different combinations of cells, biomaterials, and scaffolds have successfully generated 3D EHTs (***Seguret et al.*** (***2021***); ***Zhuang et al.*** (***2022***)) with various geometries including spheroids

(**Beauchamp et al.** (**2015**); **Polonchuk et al.** (**2017**); **Giacomelli et al.** (**2020**); **Richards et al.** (**2020**); **Hofbauer et al.** (**2021**); **Lewis-Israeli et al.** (**2021**)), cardiac strips (**Hansen et al.** (**2010**); **Legant et al.** (**2009**); **Turnbull et al.** (**2014**); **Mannhardt et al.** (**2016**); **Nunes et al.** (**2013**); **Zhao et al.** (**2019**)), circular bundles (**Goldfracht et al.** (**2020**); **Tiburcy et al.** (**2017**); **Li et al.** (**2020**)), myocardium-like sheets (**Shadrin et al.** (**2017**)) or ventricle-like chambers (**MacQueen et al.** (**2018**); **Li et al.** (**2018**); **Lee et al.** (**2019**)). The EHTs are optimally formed by mixing human-induced pluripotent stem cells (hiPSC)-derived cardiomyocytes, fibroblasts, and/or other cell types such as endothelial cells to more closely mimic the structure and cellular complexity of native myocardium (**Giacomelli et al.** (**2020**); **Saini et al.** (**2015**)). However, a major obstacle in the development of EHTs is the inevitable trade-off between the need for miniaturization to increase throughput (i.e. several organoids in each well of a 96- or 384-well plate) and the biological complexity of the tissues (**Cho et al.** (**2022**)). The first EHTs were generated in small batches, using pre-designed molds, and having a millimetric size (**Boudou et al.** (**2012**); **Turnbull et al.** (**2014**); **Legant et al.** (**2009**); **Mannhardt et al.** (**2016**)). Since then, two different avenues of development have emerged. On the one hand, to optimize throughput, more straightforward, low complexity assays such as spheroids were developed to obtain smaller tissues (**Beauchamp et al., 2015**; **Polonchuk et al., 2017**). These multicellular constructs are valuable models to study drug responses and the human heart micro-environment but they lack the geometric intricacy of a native cardiac tissue. On the other hand, the search for higher tissue complexity and maturity led to the development of chambered organoids (**MacQueen et al.** (**2018**); **Li et al.** (**2018**); **Lee et al.** (**2019**)). These constructs require the use of complex techniques such as bioprinting or the use of bioreactors, and tissues are generated one at a time, making these approaches time-consuming and impractical on a large scale. Therefore, the next step in tissue engineering needs to be directed towards high-throughput physiologically-relevant assays that are simple and straightforward for the end-user. Scaling down the tissue size to increase throughput, while controlling their geometry represents a major engineering challenge. Moreover in actual designs, many EHTs are attached on static posts that can impact tissue formation, result in isometric contraction and can interfere with optical acquisitions when made with opaque material.

Here, we report the development of a novel assay which allows fast, reproducible and high-throughput generation of 3D cardiac rings in a 96-well plate using hiPSC-derived cardiomyocytes. The design allows the formation of multiple ring-shaped cardiac tissues in a well. The EHTs form around a central pillar made from an optically-transparent and deformable polymer that enables *in situ* monitoring of the tissue contraction with simultaneous measurements of force generation.

Results

Design and characterization of the molds

3D steel molds were designed to obtain a structure on which cells can be directed to ring-shaped cavities during sedimentation (Figure 1A). The mold fits in the well of a 96-well plate, and consists of 21 identical conical structures with a central hole (Figure 1A left). The molds obtained from the manufacturer were imaged by scanning electron microscopy and found to correspond to the intended design (Figure 1A, right). Casts of the mold were created in PEG to check the shape of the inner cavities of the mold, but the resulting structures were too soft to maintain their shape in air, and were transparent in water and therefore could not be imaged. More rigid polydimethylsiloxane (PDMS) was cast from the mold to verify the shape of the resulting structures (Figure 1B). These showed that the interior profile of the cavity was shaped in a reversed hourglass, as expected.

Generation and characterization of the gels

3D gel structures were obtained by adding a drop of PEG gel solution on top of the molds, inverting these onto a glass coverslip, polymerizing the gel and attaching the resulting sample on a 96-well plate. To determine the stiffness of the gels, a sample of the aqueous PEG solution was polymerized. A capillary was placed perpendicularly to the edge of the gel and negative pressure was applied to the gel through the capillary. The deformation of the gel into the capillary was measured and used to determine the Young's modulus of the gel (Figure 1 supplement 1). The values obtained (11.4± 0.5 kPa) are within the physiological range for human cardiac tissue (**Gershlak**

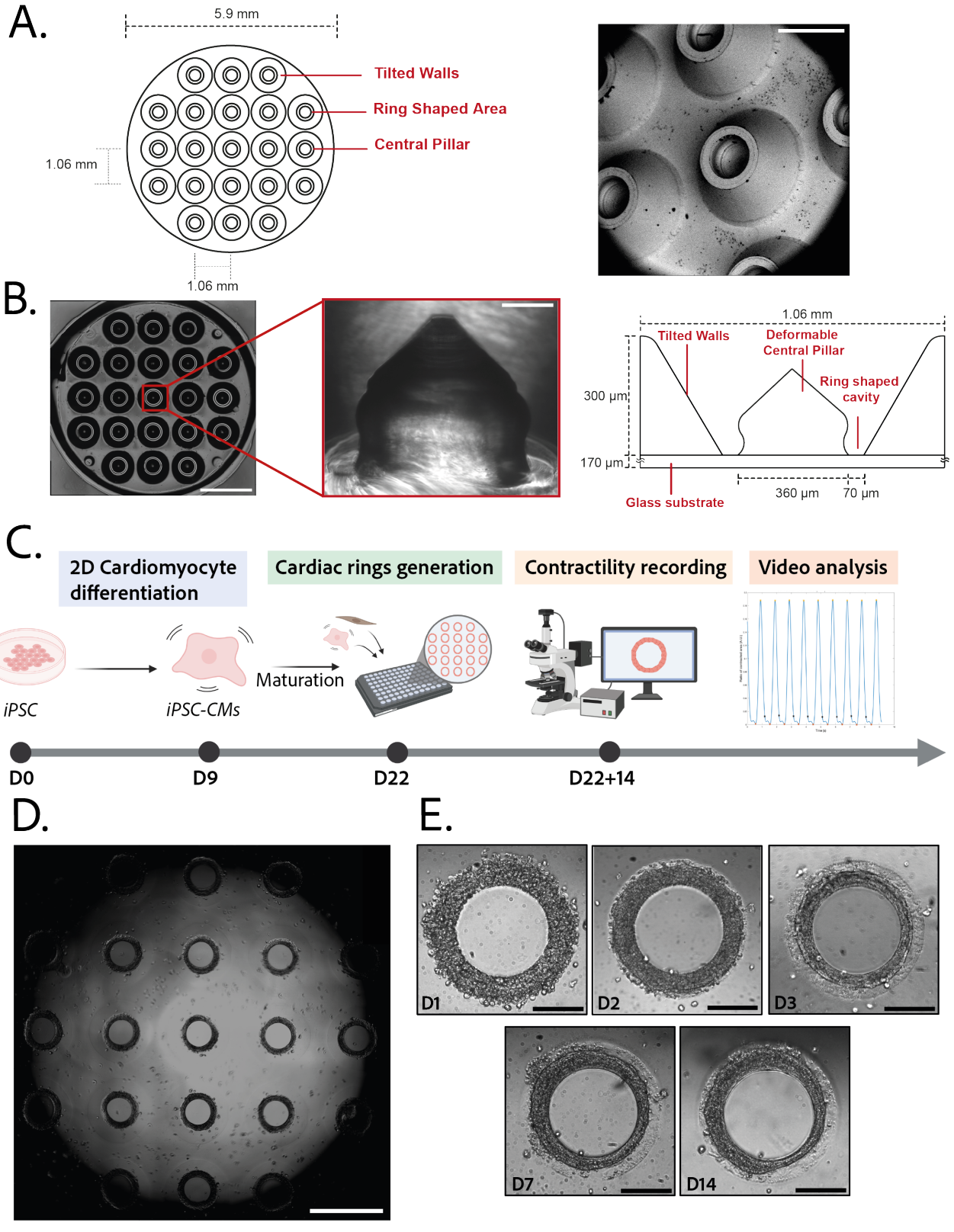

Figure 1. Description of the mold and seeding procedure. **A.** Micromachined stainless steel mold used to shape the gel – Design (left) and scanning electron microscopy image (right) of the mold – Scale bar: 500 µm. **B.** Molded PEG gel (left - scale bar 2 mm) and zoomed view of a pillar from its PDMS replica (middle- scale bar 100 µm). Design and size of the pillar (right). **C.** Timeline of the seeding procedure. **D.** Cardiac rings in a well one day after seeding. Images stitched with ImageJ plugin - Scale bar: 1 mm. **E.** Representative compaction of a ring with time after seeding (from day 0 to day 14), in brightfield - Scale bars: 200 µm.

Figure 1—figure supplement 1. Measurement of the Young's Modulus of PEG gel

Figure 1—figure supplement 2. Measurement of the efficiency of differentiation the the iPSCs into cardiomyocytes.

Figure 1—video 1. Multiple rings beating at D14 - Brightfield imaging x4 magnification.

et al. (*2013*)).

Generation of ring-shaped cardiac tissues

The efficiency of the differentiation of iPSCs into cardiomyocytes was in average of 96.9 ± 0.8 % (Figure 1 Supplement 2).Cardiomyocytes derived from iPSCs (iPSC-CMs) with fibroblasts were seeded on the gels. After centrifugation, the cells sedimented into the ring-shaped cavities (Figure 1D), and compacted around the pillars to rapidly form ring-shaped cardiac constructs (Figure 1D-E). Initial tests with cardiomyocytes resulted in cell cluster formation and malformation of the rings (Figure 2A). To stabilize the tissues, iPSC-CMs were mixed with fibroblasts and different ratios of hiPSC-CMs to fibroblasts were tested in order to obtain the highest number of full stable cardiac rings with time. Three ratios of hiPSC-CMs:fibroblasts were tested (Figure 2B) based on previous reports (*Tiburcy et al.* (*2017*); *Saini et al.* (*2015*); *Giacomelli et al.* (*2020*); *Beauchamp et al.* (*2020*)). The 3:1 hiPSC-CMs:fibroblasts ratio was determined to be optimal and was used for all of the following experiments. Tissues started beating within 24 hours after seeding (Video 1). The rings compacted in time as shown in Figure 1E. In these optimization experiments, we obtained an average of 10.75±0.48 tissues per well which were stable over time for at least 20 days with the 3:1 hiPSC-CMs:fibroblasts ratio.

Structure and organization of the engineered cardiac tissues

The 3D organization of the tissues was assessed by 3D immunofluorescence imaging 14 days after seeding. The fibroblasts are concentrated at the base of the ring in contact with the glass (Figure 2C – bottom panel), whereas the cardiomyocytes form a compact ring above the fibroblasts around the central pillar (Figure 2C – top panel). Troponin T staining evidenced the formation of striated elongated fibers (Figure 2D), which are typical of cardiac tissue. The obtained cardiac tissues are 75.5±1.8 µm high and their shape is toric, as shown in the 3D reconstruction (Figure 2E and video 1).

Contractility analysis

Tissues started contracting less than 24 hours after seeding, which was visible through the deformation of their central pillar (Supplemental video 1). Each tissue was recorded in brightfield imaging, at a 10X magnification with a high-speed camera (Supplemental video 1). An in-house Matlab code was developed to quantify the contraction and relaxation phases of the tissues by monitoring the area of the central pillar over time (Figure 3A). The beat rate of the tissues first decreased between day 1 and day 3 and increased again to reach 0.58±0.030 Hz on day 14 (Figure 3B). The contraction stress developed by the tissues increased from day 1 until day 7 (Figure 3C). At day 7, the contractility parameters stabilized with an average stress of 1.4±0.1 mN/mm^2 (Figure 3C.). The corresponding developed strain ϵ_A was of 24.84±0.92 % (Figure 3 supplement 1). Consistently, the relaxation and contraction speeds also increased during the first 7 days, then reaching a plateau (Figure 3D and E).

Physiological testing on the engineered cardiac tissues

The response in contractility of the cardiac rings to an increase in the extracellular calcium concentration was assessed by sequential addition of calcium in the medium, starting from a concentration of 0.5 mM up to 3.5 mM (Figure 4A). The changes in the contraction stress and the contraction and relaxation speeds with calcium concentration were significant ($p<0.0001$ for each parameter, non significant for the beat rate). We observed a stabilization of the beat rate around 0.5Hz at 2mM and a positive inotropic response as the contraction amplitude increased by 600 % with a corresponding EC_{50} of 1.346 mM with a confidence interval (CI) of [1.159;1.535] mM.

Pharmacological testing on the engineered cardiac tissues

We next evaluated the dose-response to increasing concentrations of several cardiotropic drugs. The changes in the beating parameters with verapamil concentration were found to be significant ($p=0.0053$ for the beat rate and $p<0.0001$ for the other parameters). The addition of verapamil, an L-type calcium channel inhibitor, induced a negative inotropic effect until the com-

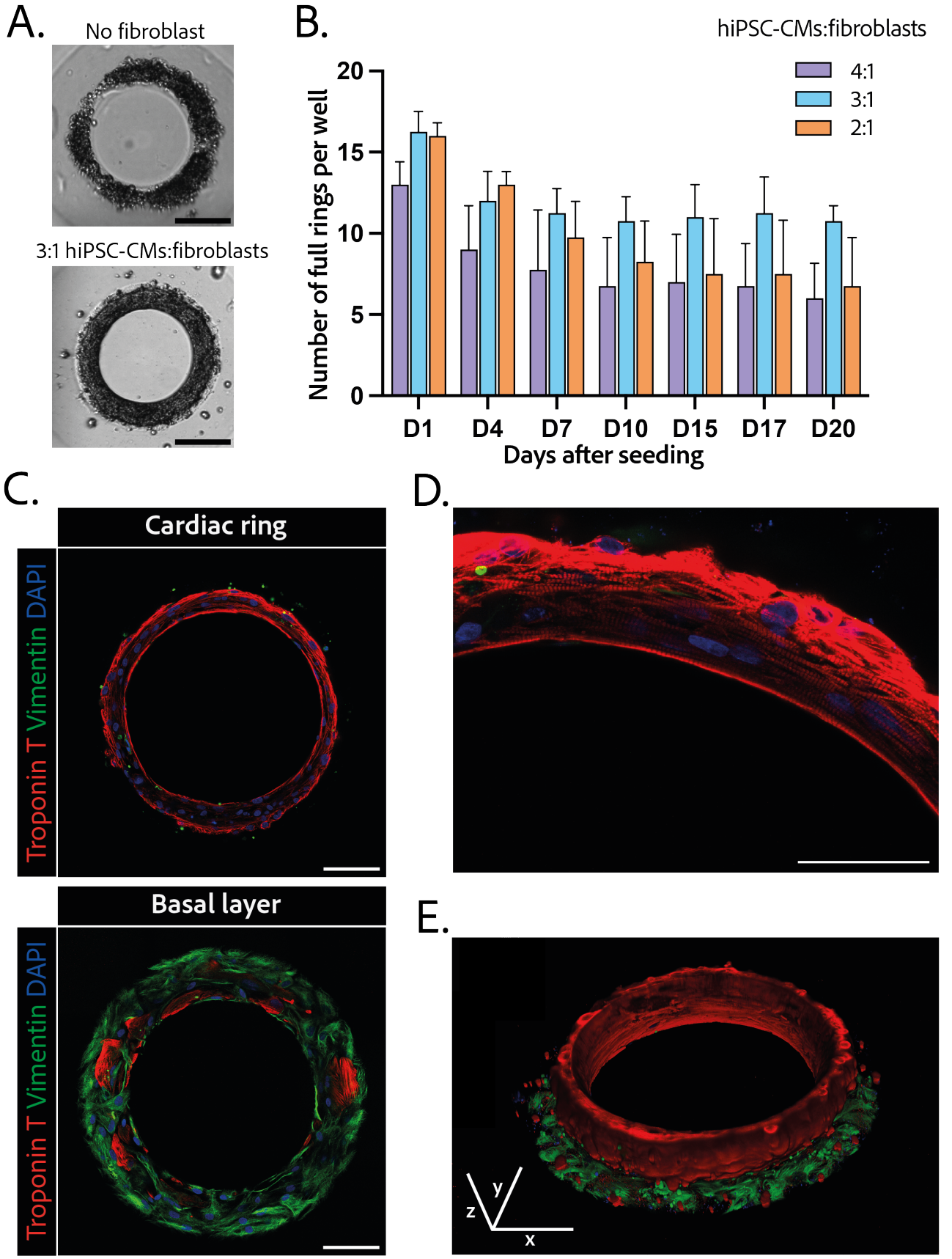

Figure 2. Composition and structure of the cardiac rings. **A.**Example brightfield images of cardiomyocytes seeded with or without fibroblasts one day after seeding - Scale bar : 200 µm. **B.**Number of full cardiac rings per well in time according to the hiPSC-CMs:fibroblasts ratio they contain (4:1, 3:1 or 2:1). **C.**Confocal imaging of immunostained tissues at different heights: cardiac ring (top panel), and basal layer (bottom panel) of a tissue at 40X magnification. Vimentin, stained in green, corresponds to fibroblasts, troponin T, in red, is specific to cardiomyocytes, and DAPI is in blue. Scale bars: 100 µm. **D.**Picture of the immunostained contractile fibers at 63X magnification. Vimentin (green), Troponin T (red) and DAPI (blue) – Scale bar: 50µm. **E.**3D reconstruction of a ring. x, y and z scale bars : 100 µm.

Figure 2—figure supplement 1. Larger scale pictures of panel C.

Figure 2—video 1. 3D reconstruction of a ring

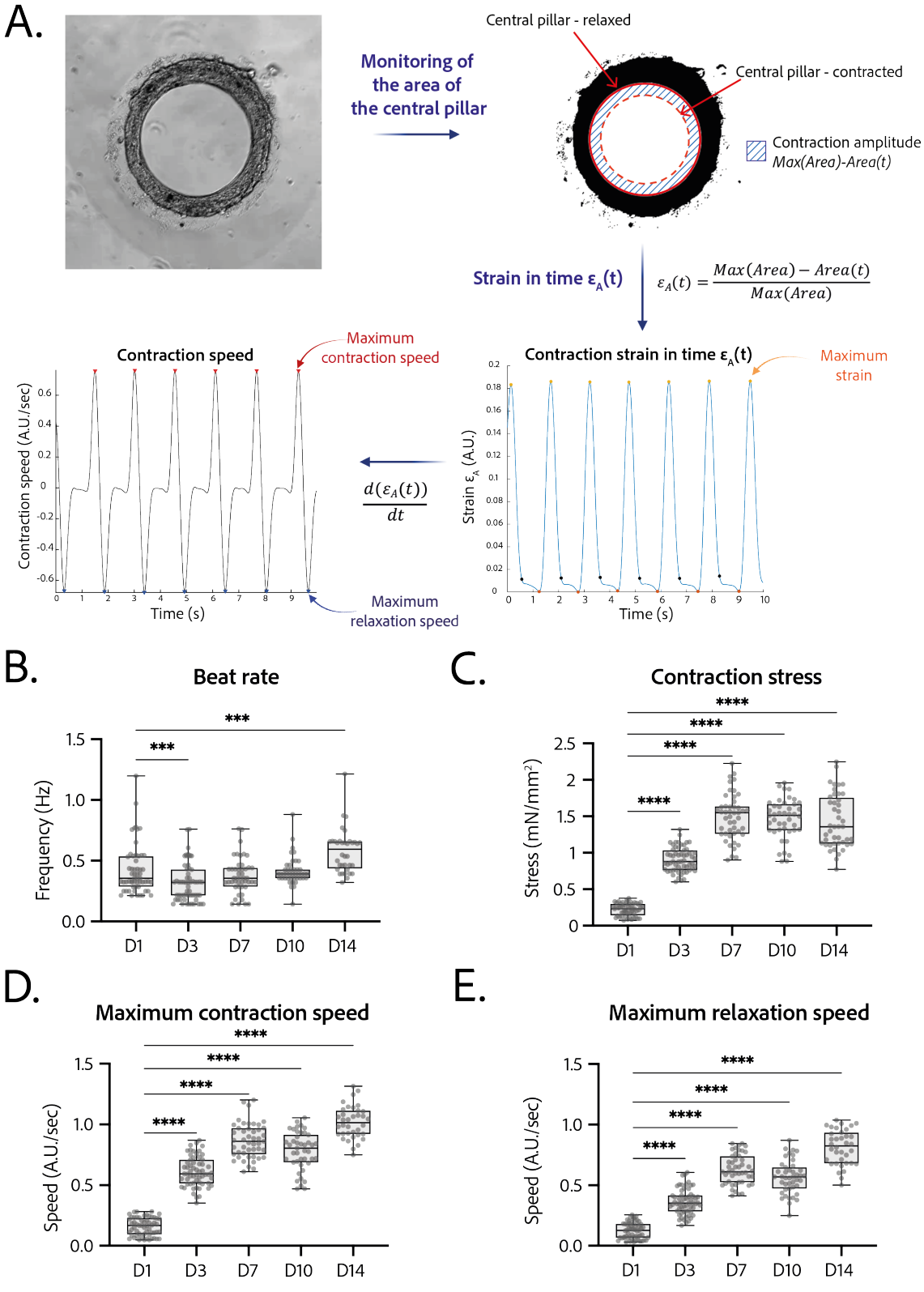

Figure 3. A. Principle of the in-house Matlab code used for contractility analysis: detection of the central pillar and monitoring of the evolution of its area in time, calculation and plot of the strain ϵ_A in time (ratio between the contraction amplitude in time and the maximum area of the central pillar) – Representative plots of the strain in time and its derivative in time, for a tissue at day 14. **B. to E.**Evolution of beating parameters through time after seeding at days 1, 3, 7, 10 and 14. The changes of all the parameters through time are significant (p<0.0001 - ANOVA for repeated measures -D1: n=57, D3: n=59 D7: n=47, D10: n=43, D14: n=36 tissues, from 3 differentiations). Beating parameters at each time point are compared to their value at day 1. **B.** Evolution of beat rate through time after seeding (***: p<0.002). **C.**Evolution of contraction stress through time after seeding (****: p<0.0001). **D.**Evolution of maximum contraction speed through time after seeding (****: p<0.0001). **E.**Evolution of maximum relaxation speed through time after seeding (****: p<0.0001).

Figure 3—figure supplement 1. Strain ϵ_A developed by the rings at D14.

Figure 3—video 1. Contractility of a ring at day 14.

plete stop of contraction at 10µM, as expected (Figure 4B). The IC_{50} was estimated to be 0.677 µM, CI=[4.278;12.81].10^7 M. The dose-response to the β-adrenergic receptor agonist, isoproterenol was tested. We observed a trend towards increase of the contraction amplitude, as well as a significant increase in the contraction and relaxation speeds (Figure 4C), without change in the beat rate. The changes in the contraction stress and the contraction and relaxation speeds with isoproterenol concentration are significant (p=0.0004 for the contraction stress; p<0.0001 for the contraction and relaxation speeds). Finally, dofetilide, which is an inhibitor of the I_{Kr} current, was also tested at different concentrations on the cardiac rings. This drug has been shown to be pro-arrhythmic and to induce arrhythmic events such as Torsades-de-Pointes in patients. The changes in the beat rate, the contraction stress and the contraction and relaxation speeds with dofetilide concentration were found to be significant (p<0.0001 for all the parameters). As shown in Figure 4D, dofetilide significantly reduced the contraction stress and speeds until the complete stop of the contraction of the cardiac tissues for a concentration of 10 nM. Arrhythmic events were noted after adding dofetilide at concentrations of 3 and 7 nM. Indeed, the Poincaré diagram for the different dofetilide concentrations (Figure 4E) shows an increase in the contraction-to-contraction intervals (equivalent to RR intervals) for some cells at 1 nM of dofetilide and an increasing number of erratic beats with increasing dofetilide concentrations.

Discussion

The combination of pluripotent stem cells technologies, advanced cardiomyocyte differentiation protocols and microfabrication methods have already resulted in the generation of engineered human cardiac muscle tissue-constructs, with different shapes and that can reproduce some cardiac functions (***Seguret et al.*** (***2021***); ***Cho et al.*** (***2022***)). However, until now, approaching the complex geometry and structure of the human myocardium required complex techniques, which limits the number of tissues produced, thus hampering their application for high-throughput experiments. In this study, we aimed to address this challenge by developing a novel strategy to create ring-shaped miniature cardiac tissues around a central pillar that is made from an optically-transparent and deformable polymer. Our main findings are as follows : (1) this novel strategy enables the fast and reproducible formation of an important number of cardiac tissues (up to 21 per well in a 96-well format) with a limited number of hiPSC-cardiomyocytes (112,500 per well); (2) In this assay, fibroblasts are essential to generate and maintain the tissue structure, with a 3:1 hiPSC-CMs:fibroblast ratio providing with the best yield of tissue generation; (3) The self-organized ring-shaped cardiac tissues contract and deform the optically-transparent central pillar, which can be recorded and analyzed to estimate the contractile force developed by the tissue; (4) these EHTs display concordant responses to positive or negative inotropes, and to arrhythmogenic drugs, as required for drug testing applications.

The miniaturized cardiac constructs develop by self-organization of the hiPSC-derived cardiomyocytes and fibroblasts, which are guided by a specific design to acquire a ring shape. The resulting EHTs are in a convenient 96-well plate format and easy to use for a user familiar with cell biology techniques. The 96-well plate format is adaptable to many plate readers and automated platforms. In addition, the optical clarity of the gels and the absence of gel directly under the structures ensures optimal imaging conditions. We showed that the tissues can be fixed, stained by immunofluorescence and imaged in situ at high resolution. Moreover, our EHTs would also be compatible with live cell imaging experiments with fluorescent reporters, such as calcium transients studies or conduction studies by optical mapping. While imaging the fluorescent reporter, the contraction parameters could be monitored through the deformation of the pillar. The possibility to simultaneously record two parameters represents a significant asset. The current design of our EHTs consists of up to 21 rings in a single well, thus providing many replicates within a single experiment, even if some of the rings fail to form due to biological variability. This high throughput can compensate for potential intra-batch effects. Moreover, the possibility to seed several wells at the same time allows to easily study several differentiations, compensating for the variability which is inherent to the differentiation of hiPSCs. The predictable circular shape of the tissues makes them easy to recognize and track using software. Coupled with the known organization of the 21 rings

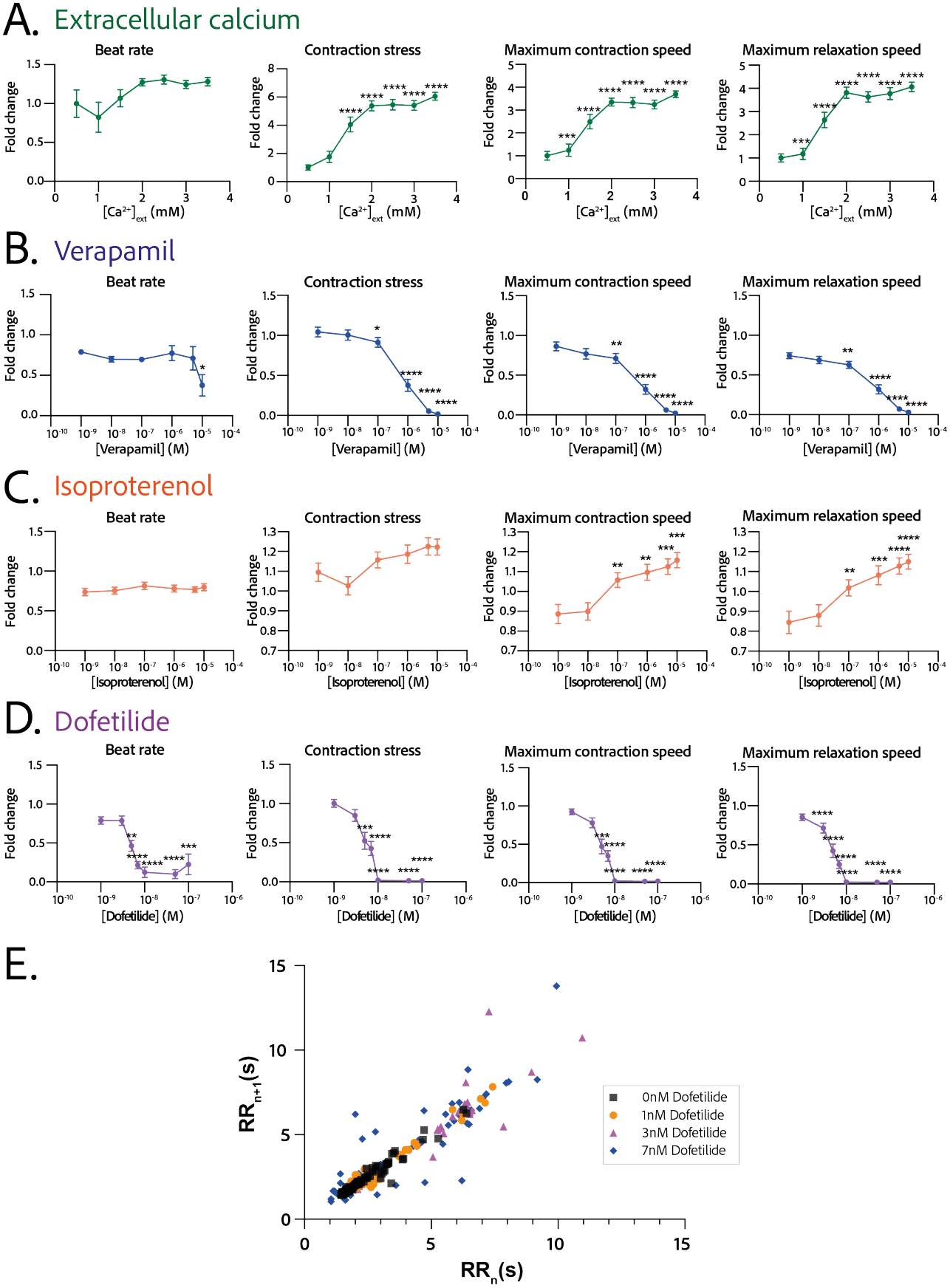

Figure 4. Physiological and drug testing on the cardiac tissues. Effect of the concentration in extracellular calcium (**A.**), verapamil (**B.**), isoproterenol (**C.**) or dofetilide (**D.**) on tissues contractility: beat rate, contraction stress and the maximum contraction and relaxation speeds. These parameters are expressed as a ratio between their value for each concentration and the value at basal state ($[Ca^{2+}]$=0.5 mM for calcium test and [Drug]=0M for drug testing). An ANOVA for repeated measures was carried out for each parameter. For each test, the value of each parameter at each concentration is compared to its value at the minimal concentration of the drug (respectively [Ca2+]=0.5mM, [Verapamil]=10^{-9} M, [Isoproterenol]=10^{-9} M and [Dofetilide]=10^{-9} M). **E.** Poincaré plot for 0 nM, 1 nM, 3 nM and 7 nM of dofetilide. For each concentration of each drug, more than 20 tissues from 3 different concentrations could be analyzed. Data is presented as mean ± SEM. *: p<0.05; **: p<0.01; ***: p<0.001; ****: p<0.0001.

for easy automated imaging, a single well can quickly generate data on many tissues that is quickly and automatically analyzed. The EHTs we described here are thus easy to use, image, manipulate and obtain readouts from.

We found that the circular geometry of these self-organized cardiac tissues induces a homogeneous distribution of the cardiomyocytes and consequently of the contraction forces around the pillar and in the tissue. Importantly, the presence of the central pillar not only allows resistance to be felt by the tissue, but the control of its stiffness facilitates the calculation of the force developed by the tissue. Our results showed that the tissues develop a fractional shortening (or contraction strain) of about 25%, which is close to the contraction of a human heart (***Cheng et al.*** (***2010***)). The corresponding stress was 1.4 mN/mm^2 which is in a similar range to other previously reported tissue-engineered cardiac muscle models with hiPSC-CMs in the literature (***Seguret et al.*** (***2021***); ***Turnbull et al.*** (***2014***); ***Shadrin et al.*** (***2017***); ***Zhao et al.*** (***2019***); ***Ronaldson-Bouchard et al.*** (***2018***); ***Goldfracht et al.*** (***2020***); ***Li et al.*** (***2020***)). Some studies have reported higher force values (***Ronaldson-Bouchard et al.*** (***2018***)) but in tissues that have a much large size than the tissues proposed here. The force generated by the adult human heart muscle, around 44 mM/mm^2 for a tissue strip (***Hasenfuss et al.*** (***1991***)), however remains significantly higher than the force developed by the currently available platforms. Few cardiac assays can precisely monitor the force exerted by the tissues. Indeed, cardiac cells seeded on micropillars (***Rodriguez et al.*** (***2014***)) and gels containing tracking beads (***Dou et al.*** (***2021***); ***Feyen et al.*** (***2020***)) can provide information on local (subcellular) force exertion. The force measurements do not result from the concerted effort of an organized tissue composed of aligned cardiomyocytes, as proposed by ring-shaped tissues. Tissues attached on two posts (***Turnbull et al.*** (***2014***); ***Mannhardt et al.*** (***2016***); ***Abilez et al.*** (***2018***)) can also provide some information on the force generated by a tissue but the force exertion is not radial as it is in the native heart and the presence of the posts can impact the contraction by affecting the force distribution in the tissue and creating potential edge effects in the vicinity of the posts, inducing the formation of v-necks (***Abilez et al.*** (***2018***)). Lastly, some other ring-shaped cardiac constructs have to be transferred on posts or on a force transducer to measure their contraction force (***Goldfracht et al.*** (***2020***); ***Tiburcy et al.*** (***2017***)). Therefore, the easy *in situ* monitoring of the force generated by our ring-shaped tissues with an image analysis routine represents a significant advantage, as less manipulation improves the degree of standardization. Finally, the stiffness of the central pillar can easily be adapted to model a pathological increase or decrease of the extracellular matrix stiffness.

The EHTs we developed are composed of cardiomyocytes that rely on fibroblasts for their assembly and inter-cellular adhesion. Fibroblasts have been shown to play a prominent role in the heart as they are crucial in the constitution of the supporting extracellular matrix and contribute to cardiomyocyte electrical coupling, conduction system insulation, vascular maintenance, and stress-sensing (***Ivey and Tallquist*** (***2016***); ***Baudino et al.*** (***2006***)). Other studies have highlighted the importance of a multi-cellular approach to generate EHTs (***Giacomelli et al.*** (***2020***); ***Saini et al.*** (***2015***); ***Amano et al.*** (***2016***); ***Caspi et al.*** (***2007***)). In our system, the fibroblasts additionally play a role in providing a basement support under the cardiomyocytes, in contact with the glass support of the EHTs. Immunofluorescence imaging showed an organization of the cardiomyocytes parallel to each other, perpendicular to the direction of contraction, with an increased alignment of sarcomeres. Our EHTs mimic the composition and organization of the native myocardial tissue, even if only composed of cardiomyocytes and fibroblasts. Future experiments will determine whether other, less abundant, cell types of the native myocardium, such as endothelial or smooth muscle cells, can further improve heart tissue modeling.

The constructs showed a spontaneous beating in the day following seeding and this activity was maintained over several weeks thus allowing contractile measurements and pharmacological testing in the conditions of auto-pacing. As a proof-of-concept, we studied the effects of well-established negative and positive inotropes and showed the ability of our platform to reproduce the anticipated effects. We observed that our tissues presented a positive inotropic response to increasing extracellular calcium concentration with a corresponding EC_{50} which is in agreement with the values reported in the literature for engineered heart tissues made of hiPSC-CM, which are between 0.4 and 1.8mM for the EC_{50} (***Feric and Radisic*** (***2016***); ***Schaaf et al.*** (***2011***); ***Streckfuss-***

Bömeke et al. (***2013***); ***Mannhardt et al.*** (***2016***); ***Turnbull et al.*** (***2014***); ***Goldfracht et al.*** (***2020***)). The negative inotropic response to increasing concentrations of verapamil of our constructs was also described in the literature and our IC_{50} value is also in the range of reported values in other EHTs: Turnbull et al. ***Turnbull et al.*** (***2014***) found IC_{50}=0.61 µM and other papers range from 0.3 µM to 0.6 µM (***Mannhardt et al.*** (***2016***); ***Thavandiran*** (***2019***)). The β-adrenergic stimulation of the tissues with increasing concentrations of isoproterenol-induced a trend towards increase in the contraction force and significantly increased contraction and relaxation speeds without change in the beat rate. This is in line with what has been shown by ***Goldfracht et al.*** (***2020***) and ***Zhao et al.*** (***2019***). Last, applying increasing dofetilide concentrations on our constructs showed a decrease in the contraction amplitude and contraction and relaxation speeds. This is in line with the literature as Zhao et al. ***Zhao et al.*** (***2019***) depicted a significant reduction of the action potential amplitude of the tissues above a concentration of dofetilide of 10 nM. By assessing the beating regularity by plotting each period as a function of the previous one, we highlighted an increasing number of erratic beats with the increase in dofetilide concentration. Other papers have also underlined the pro-arrhythmic effect of dofetilide on cardiomyocytes derived from iPSCs (***Goldfracht et al.*** (***2019***); ***Patel et al.*** (***2019***); ***Altrocchi et al.*** (***2020***); ***Blinova et al.*** (***2017***)). Therefore, we demonstrated that our platform recapitulated the expected cardiac responses to several inotropes and arrhythmogenic drugs.

While representing a significant improvement, our platform presents some limitations. First, the size of the rings is very small compared to native tissue (400 µm). This size limitation is necessary for the purposes of high throughput screening, but for applications requiring larger tissues, wider rings can be considered in the future. Second, all measurements were performed under spontaneous pacing as a specific technique should be developed to allow external pacing of the tissues in the 96-well format. This includes electrical field stimulation or an optogenetics system with light stimulation. The precise and regular organization of the rings in the well makes this design very amenable to the introduction of microelectrodes for pacing, which could also allow the measurement of the action potentials of individual micro-tissues. Nevertheless, our main results show that pharmacological responses, including the detection of the pro-arrhythmogenic effects of dofetilide, were correctly measured under spontaneous beating conditions. Third, the miniaturized format of our platform creates some limitations and challenges regarding some experiments, including tissue stretching. Therefore, the length-tension relationships (Franck-Starling mechanism) were not determined in our tissues.

Overall the novel platform we describe here is a versatile, easy-to-use and high-throughput tool to generate cardiac rings in a reproducible way and analyze them *in situ*. This platform will be useful in several cardiac research fields, including disease modeling and pharmacological testing.

Methods and Materials

Mold design and characterization

Micromachined stainless steel molds were obtained from high resolution CNC machining according to our CAD designs. The designs consisted of a mold that would be slightly smaller than the footprint of a well of a 96-well plate, composed of 21 structures (see Figure 1A). To check the shape of the interior cavities of the mold, a cast of the mold was created out of polydimethylsiloxane (PDMS) (Sylgard 184, Samaro), according to manufacturer's instructions.

3D hydrogel substrate preparation

A solution of 5% w/w photopolymerizable polyethylene glycol (PEG) was prepared in distilled water. Circular coverslips (16 mm, Paul Marienfeld GmbH, Germany) were silanized to ensure adequate bonding between the PEG and glass. A drop of 10-15 μL of gel was placed on the stainless steel mold, which was then placed in contact with a silanized coverslip. The gel solution was briefly exposed to light of the appropriate wavelength to polymerize the hydrogel. The resulting 3D structured hydrogel, bound to the coverslip, was unmolded and immediately placed in distilled water. The hydrogel was rinsed at least three times with distilled water and incubated in water overnight. For cell experiments, the coverslip coated in a 3D hydrogel was briefly dried and attached to a

commercial black polystyrene 96-well plate with an adhesive backing (Grace Bio-labs, USA). The resulting well was filled with distilled water. Prior cell seeding, the plate was sterilized by UV irradiation for at least 20 minutes.

Young's modulus measurements of the molds

The PEG-based hydrogel solutions were prepared and 100µL of solution was deposited into a ring-shaped mold with an inner diameter of 1cm positioned on a 16mm glass coverslip. The solution was polymerized using 365nm UV light for 1 minute at a power of 70 mW/cm^2, after which the mold was removed. The coverslip containing the gel was then transferred to the microscope (Leica camera AG, Germany). A hollow glass capillary with an inner diameter 0.75mm (World Precision Instruments, USA) was attached to a platform movable in the xy-plane which was used to position the capillary right next to the edge of the circular polymerized hydrogel. Once the capillary and the hydrogel made contact, a negative pressure was applied, using the Cobalt autonomous pressure pump (Elvesys, France), creating a small convexity in the surface of the hydrogel. Images of this convexity were taken (5X magnification) for a pressure ranging from -100mbar to -200mbar, with 10 mbar increments (Figure 1A.). Two measurements were done on two separate gels, resulting in 4 measurements per gel with 10 datapoints each. The images (and thus the size of the convexities) were analyzed using ImageJ (version 1.53c). The Young's modulus was calculated with the formula $E = \frac{p}{0.872\frac{l}{a}+0.748(\frac{l}{a})^2}$ according to literature (***Gandin et al.*** (***2021***)).

Cardiomyocyte differentiation and culture

The SKiPSC-31.3 hiPSC cell line, from a healthy control subject, has been used here and was previously reported (***Galende et al.*** (***2010***)). Induced pluripotent stem cells were seeded on Matrigel and cultivated in mTESR Plus medium (Stemcell Technologies). At 80 % confluency, cells were passaged with ReleSR reagent (StemCell Technologies). When hiPSCs reached a 90 % confluency, differentiation was carried out according to a protocol adapted from ***Garg et al.*** (***2018***). Briefly, on day 0 of differentiation, mTESR Plus was changed to RPMI-1640 (Life Technologies) supplemented with B27 without insulin (RPMI-B27 minus insulin) and 6 µM CHIR-99021 (Abcam). After 48 hours, the medium was changed to RPMI-B27 minus insulin and then to RPMI-B27 minus insulin with 5µM IWR-1 (Sigma) for 48 hours. On day 5, the medium was replaced by RPMI-B27 minus insulin, and switched to RPMI-B27 with insulin on day 7. At day 11 a glucose starvation was carried out by replacing the medium with RPMI 1640 without glucose (Life Technologies), supplemented by B27 with insulin for 3 days. Cells were then dissociated with 0.05% trypsin (Life Technologies) and re-plated in a 12-well plate at a density of 0.3 10^6 cells/cm^2 in RPMI-B27 with insulin. The following day, the medium was switched back to RPMI 1640 without glucose (Life Technologies), supplemented by B27 with insulin for 3 days again. These two rounds of glucose starvation have been shown to increase dramatically the percentage of cardiomyocytes obtained ***Sharma et al.*** (***2015***). After day 18, the cells were cultured in RPMI-B27 with insulin and the medium was changed every two days.

Cardiomyocyte characterization

The efficiency of the differentiation was assessed by cardiac troponin T flow cytometry at D21. On day 21 of differentiation, hiPSC-CMs were dissociated by enzymatic digestion (Miltenyi Multi Tissue dissociation kit 3) and stained with the Zombie NIR™ Fixable Viability Kit (BioLegend). Then, collected cell pellets were fixed and permeabilized using Inside Stain kit (Miltenyi Biotech, 130-090-477) at room temperature for 10 minutes. Cells were incubated with either APC anti-cardiac troponin T (CTNT) antibody (Miltenyi Biotech; 130-106-689 1:100) or APC isotype control (Miltenyi Biotech, 130-104-615 1:100) for 10 min at room temperature. Cells were analyzed using the BD Biosciences FACS LSR Fortessa X-20 instrument with at least 30,000 cells. Results were processed using FlowJo v10 (FlowJo, LLC).

Human fibroblasts culture

Commercially available normal adult human dermal fibroblasts (NHDF-Ad Lonza CC-2511, Lot 545147) were used up to passage 6 to generate the tissues. They were cultured in T75 flasks, in DMEM high glucose, supplemented with 10% FBS, 1% NEAA and 1% penicillin-streptomycin.

Tissues generation and culture

The wells of the assay were first rinsed twice with PBS and incubated at 37°C in DMEM high glucose, 2.3 mM CaCl2, 10%FBS, 0.1% penicillin-streptomycin. To generate the tissues, cardiomyocytes were dissociated by enzymatic digestion (Miltenyi Multi Tissue dissociation kit 3) on day 22 after differentiation. Fibroblasts were dissociated with TrypLE Express Enzyme (12605010 Thermofischer). Three ratios of hiPSC-CMs:fibroblasts were tested: 4:1, 3:1 and 2:1. For the following experiments the tissues are generated with a ratio of 3:1 hiPSC-CMs:fibroblasts as this ratio allowed the best preservation of tissues in time. A total of 150k cells were seeded in each well. The required numbers of fibroblasts and cardiomyocytes were then mixed and resuspended in 200µL per well of DMEM high glucose, 2.3 mM CaCl2, 10%FBS, 0.1% penicillin-streptomycin. The plate was then incubated at 37°C for 5 minutes and centrifuged 3 times in "short" mode to ensure that the cells fall into the circular molds. The plate was then kept at 37°C and the medium was changed every two days.

Tissues recording and analysis

The cardiac rings were recorded for 10 seconds in brightfield imaging with a high speed CCD camera (PL-D672MU, Pixelink) mounted on a microscope (Primovert, Zeiss), at a 10X magnification. The videos were then analyzed with a custom Matlab script. Briefly, the area of the central pillar is monitored in time and allows to recover the contraction amplitude in time Amplitude(t)= Max(Area)-Area(t) and therefore the contraction strain in time (in terms of area) ϵ_A calculated as $\epsilon_A(t) = (Max(Area) - Area(t))/Max(Area)$ as well as the derivative of this strain in time. $\epsilon_A(t)$ is linked to the linear strain ϵ with the formula $\epsilon = \frac{\Delta r}{r_{max}} = \frac{\epsilon_A}{1+\sqrt{1-\epsilon_A}}$. As we measured the Young's Modulus of the gel, we can recover the stress developed by the cardiac rings $\sigma = E.\epsilon(t)$. From these traces we also derive the contraction frequency by Fourier transform. It was considered that below a contraction of 0.5 %, the signal to noise ratio was not sufficient enough to detect the contraction of the tissue and the beating frequency was therefore set to 0 Hz. Finally, the maximum contraction and relaxation speeds of the tissue were also calculated respectively from the maxima and minima of the derivative of this strain in time.

Response to increasing extracellular calcium concentration and drug tests

Tissues response to different drugs and increasing calcium concentrations was assessed after day 14. For the increasing extracellular calcium concentrations, tissues were first changed to Tyrode solution 0.5 mM in calcium (NaCl 140 mM, KCl 5 mM, 10 mM Hepes, Glucose 10 mM, $MgCl_2$ 1 mM, $CaCl_2$ 0.5 mM, pH 7.4) and let to equilibrate for 30 minutes at 37°C, 5 % CO2. Calcium concentration was then increased by sequential addition of a Tyrode solution at 10mM in calcium. After each addition, the tissues were incubated for 5 minutes before recording. For drug tests, tissues were changed to Tyrode solution at 1.8mM in calcium (NaCl 14 mM, KCl 5 mM, 10 mM Hepes, Glucose 10 mM, $MgCl_2$ 1 mM, $CaCl_2$ 1.8 mM, pH 7.4) and let to equilibrate for 30 minutes at 37°C, 5% CO2. To evaluate the dose-response of the cardiac rings to the different drugs (Verapamil- sigma v0100000, isoproterenol - sigma 1351005, dofetilide - sigma PZ0016), the contractility was first recorded for 30 seconds in basal state and the drug was then added sequentially. Between each addition of drug, the tissues were incubated for 5 minutes at 37°C before being recorded for 30 seconds.

Immunofluorescence staining and confocal microscopy

Tissues were fixed at day 15 with 4% paraformaldehyde for 15 minutes and rinsed 3 times in PBS for 5 minutes. They were then blocked and permeabilized with blocking solution(BSA 2%, Triton 0.5%) at 4°C overnight. Primary antibodies Vimentin diluted at 1:250 (MA5-11883, ThermoFischer Scientific) and Troponin T diluted at 1:500 (ab45932, Abcam) were added the next day and incubated at 4°C overnight. Tissues were rinsed 3 times in PBS for 5 minutes and secondary antibodies (Alexa Fluor secondary antibodies, LifeTechnologies, at 1:1000) and DAPI diluted at 1:1000 were added and incubated at 4°C overnight. Immunostaining pictures were taken with a Leica SP8 confocal system.

Statistical analysis

All numerical results are expressed as mean ± standard error mean (SEM) of three independent experiments. Differences between experimental groups were analyzed with the appropriate statistical tests, specified each time. P values < 0.05 were considered significant for all statistical tests. Statistical analyses were performed with GraphPad Prism software.

Acknowledgments

We thank the iPS core facility of Paris Cardiovascular Research Center for its support for cell culture. We thank Camille Knops and Yunling Xu from the Flow Cytometry and the Microscopy platforms, respectively, from Université de Paris, Paris Cardiovascular Research Center, Paris, France. Schemes were created with BioRender.com (access date:10/03/2023).

References

Abilez OJ, Tzatzalos E, Yang H, Zhao MT, Jung G, Zöllner AM, Tiburcy M, Riegler J, Matsa E, Shukla P, et al. Passive stretch induces structural and functional maturation of engineered heart muscle as predicted by computational modeling. Stem cells. 2018; 36(2):265–277.

Altrocchi C, de Korte T, Bernardi J, Spätjens RL, Braam SR, Heijman J, Zaza A, Volders PG. Repolarization instability and arrhythmia by I Kr block in single human-induced pluripotent stem cell-derived cardiomyocytes and 2D monolayers. EP Europace. 2020; 22(9):1431–1441.

Amano Y, Nishiguchi A, Matsusaki M, Iseoka H, Miyagawa S, Sawa Y, Seo M, Yamaguchi T, Akashi M. Development of vascularized iPSC derived 3D-cardiomyocyte tissues by filtration Layer-by-Layer technique and their application for pharmaceutical assays. Acta biomaterialia. 2016; 33:110–121.

Baudino TA, Carver W, Giles W, Borg TK. Cardiac fibroblasts: friend or foe? American Journal of Physiology-Heart and Circulatory Physiology. 2006; 291(3):H1015–H1026.

Beauchamp P, Jackson CB, Ozhathil LC, Agarkova I, Galindo CL, Sawyer DB, Suter TM, Zuppinger C. 3D co-culture of hiPSC-derived cardiomyocytes with cardiac fibroblasts improves tissue-like features of cardiac spheroids. Frontiers in molecular biosciences. 2020; 7:14.

Beauchamp P, Moritz W, Kelm JM, Ullrich ND, Agarkova I, Anson BD, Suter TM, Zuppinger C. Development and characterization of a scaffold-free 3D spheroid model of induced pluripotent stem cell-derived human cardiomyocytes. Tissue Engineering Part C: Methods. 2015; 21(8):852–861.

Bliley JM, Vermeer MC, Duffy RM, Batalov I, Kramer D, Tashman JW, Shiwarski DJ, Lee A, Teplenin AS, Volkers L, et al. Dynamic loading of human engineered heart tissue enhances contractile function and drives a desmosome-linked disease phenotype. Science Translational Medicine. 2021; 13(603):eabd1817.

Blinova K, Stohlman J, Vicente J, Chan D, Johannesen L, Hortigon-Vinagre MP, Zamora V, Smith G, Crumb WJ, Pang L, et al. Comprehensive translational assessment of human-induced pluripotent stem cell derived cardiomyocytes for evaluating drug-induced arrhythmias. Toxicological Sciences. 2017; 155(1):234–247.

Boudou T, Legant WR, Mu A, Borochin MA, Thavandiran N, Radisic M, Zandstra PW, Epstein JA, Margulies KB, Chen CS. A microfabricated platform to measure and manipulate the mechanics of engineered cardiac microtissues. Tissue Engineering Part A. 2012; 18(9-10):910–919.

Cashman TJ, Josowitz R, Johnson BV, Gelb BD, Costa KD. Human engineered cardiac tissues created using induced pluripotent stem cells reveal functional characteristics of BRAF-mediated hypertrophic cardiomyopathy. PloS one. 2016; 11(1):e0146697.

Caspi O, Lesman A, Basevitch Y, Gepstein A, Arbel G, Habib IHM, Gepstein L, Levenberg S. Tissue engineering of vascularized cardiac muscle from human embryonic stem cells. Circulation research. 2007; 100(2):263–272.

Cheng S, Xanthakis V, Sullivan LM, Lieb W, Massaro J, Aragam J, Benjamin EJ, Vasan RS. Correlates of echocardiographic indices of cardiac remodeling over the adult life course: longitudinal observations from the Framingham Heart Study. Circulation. 2010; 122(6):570–578.

Cho S, Discher DE, Leong KW, Vunjak-Novakovic G, Wu JC. Challenges and opportunities for the next generation of cardiovascular tissue engineering. Nature Methods. 2022; 19(9):1064–1071.

Dou W, Wang L, Malhi M, Liu H, Zhao Q, Plakhotnik J, Xu Z, Huang Z, Simmons CA, Maynes JT, et al. A microdevice platform for characterizing the effect of mechanical strain magnitudes on the maturation of iPSC-Cardiomyocytes. Biosensors and Bioelectronics. 2021; 175:112875.

Eschenhagen T, Ridders K, Weinberger F. How to repair a broken heart with pluripotent stem cell-derived cardiomyocytes. Journal of Molecular and Cellular Cardiology. 2022; 163:106–117.

Feric NT, Radisic M. Towards adult-like human engineered cardiac tissue: Maturing human pluripotent stem cell-derived cardiomyocytes in human engineered cardiac tissues. Advanced drug delivery reviews. 2016; 96:110.

Feyen DA, McKeithan WL, Bruyneel AA, Spiering S, Hörmann L, Ulmer B, Zhang H, Briganti F, Schweizer M, Hegyi B, et al. Metabolic maturation media improve physiological function of human iPSC-derived cardiomyocytes. Cell reports. 2020; 32(3):107925.

Filippo Buono M, von Boehmer L, Strang J, P Hoerstrup S, Y Emmert M, Nugraha B. Human cardiac organoids for modeling genetic cardiomyopathy. Cells. 2020; 9(7):1733.

Galende E, Karakikes I, Edelmann L, Desnick RJ, Kerenyi T, Khoueiry G, Lafferty J, McGinn JT, Brodman M, Fuster V, et al., Amniotic fluid cells are more efficiently reprogrammed to pluripotency than adult cells. Mary Ann Liebert, Inc. 140 Huguenot Street, 3rd Floor New Rochelle, NY 10801 USA; 2010.

Gandin A, Murugesan Y, Torresan V, Ulliana L, Citron A, Contessotto P, Battilana G, Panciera T, Ventre M, Netti AP, et al. Simple yet effective methods to probe hydrogel stiffness for mechanobiology. Scientific reports. 2021; 11(1):1–17.

Garg P, Oikonomopoulos A, Chen H, Li Y, Lam CK, Sallam K, Perez M, Lux RL, Sanguinetti MC, Wu JC. Genome editing of induced pluripotent stem cells to decipher cardiac channelopathy variant. Journal of the American College of Cardiology. 2018; 72(1):62–75.

Gershlak JR, Resnikoff JI, Sullivan KE, Williams C, Wang RM, Black III LD. Mesenchymal stem cells ability to generate traction stress in response to substrate stiffness is modulated by the changing extracellular matrix composition of the heart during development. Biochemical and biophysical research communications. 2013; 439(2):161–166.

Giacomelli E, Meraviglia V, Campostrini G, Cochrane A, Cao X, Van Helden RW, Garcia AK, Mircea M, Kostidis S, Davis RP, et al. Human-iPSC-derived cardiac stromal cells enhance maturation in 3D cardiac microtissues and reveal non-cardiomyocyte contributions to heart disease. Cell stem cell. 2020; 26(6):862–879.

Goldfracht I, Efraim Y, Shinnawi R, Kovalev E, Huber I, Gepstein A, Arbel G, Shaheen N, Tiburcy M, Zimmermann WH, et al. Engineered heart tissue models from hiPSC-derived cardiomyocytes and cardiac ECM for disease modeling and drug testing applications. Acta biomaterialia. 2019; 92:145–159.

Goldfracht I, Protze S, Shiti A, Setter N, Gruber A, Shaheen N, Nartiss Y, Keller G, Gepstein L. Generating ring-shaped engineered heart tissues from ventricular and atrial human pluripotent stem cell-derived cardiomyocytes. Nature communications. 2020; 11(1):1–15.

Hansen A, Eder A, Bönstrup M, Flato M, Mewe M, Schaaf S, Aksehirlioglu B, Schwörer A, Uebeler J, Eschenhagen T. Development of a drug screening platform based on engineered heart tissue. Circulation research. 2010; 107(1):35–44.

Hasenfuss G, Mulieri LA, Blanchard EM, Holubarsch C, Leavitt B, Ittleman F, Alpert N. Energetics of isometric force development in control and volume-overload human myocardium. Comparison with animal species. Circulation research. 1991; 68(3):836–846.

Hofbauer P, Jahnel SM, Papai N, Giesshammer M, Deyett A, Schmidt C, Penc M, Tavernini K, Grdseloff N, Meledeth C, et al. Cardioids reveal self-organizing principles of human cardiogenesis. Cell. 2021; 184(12):3299–3317.

Ivey MJ, Tallquist MD. Defining the cardiac fibroblast. Circulation Journal. 2016; p. CJ–16.

Jabbour RJ, Owen TJ, Pandey P, Reinsch M, Wang B, King O, Couch LS, Pantou D, Pitcher DS, Chowdhury RA, et al. In vivo grafting of large engineered heart tissue patches for cardiac repair. JCI insight. 2021; 6(15).

Lee A, Hudson A, Shiwarski D, Tashman J, Hinton T, Yerneni S, Bliley J, Campbell P, Feinberg A. 3D bioprinting of collagen to rebuild components of the human heart. Science. 2019; 365(6452):482–487.

Legant WR, Pathak A, Yang MT, Deshpande VS, McMeeking RM, Chen CS. Microfabricated tissue gauges to measure and manipulate forces from 3D microtissues. Proceedings of the National Academy of Sciences. 2009; 106(25):10097–10102.

Lewis-Israeli YR, Wasserman AH, Gabalski MA, Volmert BD, Ming Y, Ball KA, Yang W, Zou J, Ni G, Pajares N, et al. Self-assembling human heart organoids for the modeling of cardiac development and congenital heart disease. Nature communications. 2021; 12(1):1–16.

Li J, Zhang L, Yu L, Minami I, Miyagawa S, Hörning M, Dong J, Qiao J, Qu X, Hua Y, et al. Circulating re-entrant waves promote maturation of hiPSC-derived cardiomyocytes in self-organized tissue ring. Communications biology. 2020; 3(1):1–12.

Li RA, Keung W, Cashman TJ, Backeris PC, Johnson BV, Bardot ES, Wong AO, Chan PK, Chan CW, Costa KD. Bioengineering an electro-mechanically functional miniature ventricular heart chamber from human pluripotent stem cells. Biomaterials. 2018; 163:116–127.

MacQueen LA, Sheehy SP, Chantre CO, Zimmerman JF, Pasqualini FS, Liu X, Goss JA, Campbell PH, Gonzalez GM, Park SJ, et al. A tissue-engineered scale model of the heart ventricle. Nature biomedical engineering. 2018; 2(12):930–941.

Madonna R, Van Laake LW, Botker HE, Davidson SM, De Caterina R, Engel FB, Eschenhagen T, Fernandez-Aviles F, Hausenloy DJ, Hulot JS, Lecour S, Leor J, Menasché P, Pesce M, Perrino C, Prunier F, Van Linthout S, Ytrehus K, Zimmermann WH, Ferdinandy P, et al. ESC Working Group on Cellular Biology of the Heart: position paper for Cardiovascular Research: tissue engineering strategies combined with cell therapies for cardiac repair in ischaemic heart disease and heart failure. Cardiovascular Research. 2019 01; 115(3):488–500. https://doi.org/10.1093/cvr/cvz010, doi: 10.1093/cvr/cvz010.

Mannhardt I, Breckwoldt K, Letuffe-Brenière D, Schaaf S, Schulz H, Neuber C, Benzin A, Werner T, Eder A, Schulze T, et al. Human engineered heart tissue: analysis of contractile force. Stem cell reports. 2016; 7(1):29–42.

Mannhardt I, Saleem U, Mosqueira D, Loos MF, Ulmer BM, Lemoine MD, Larsson C, Amèen C, de Korte T, Vlaming ML, et al. Comparison of 10 control hPSC lines for drug screening in an engineered heart tissue format. Stem cell reports. 2020; 15(4):983–998.

Nunes SS, Miklas JW, Liu J, Aschar-Sobbi R, Xiao Y, Zhang B, Jiang J, Massé S, Gagliardi M, Hsieh A, et al. Biowire: a platform for maturation of human pluripotent stem cell–derived cardiomyocytes. Nature methods. 2013; 10(8):781–787.

Patel D, Stohlman J, Dang Q, Strauss DG, Blinova K. Assessment of proarrhythmic potential of drugs in optogenetically paced induced pluripotent stem cell-derived cardiomyocytes. Toxicological Sciences. 2019; 170(1):167–179.

Polonchuk L, Chabria M, Badi L, Hoflack JC, Figtree G, Davies MJ, Gentile C. Cardiac spheroids as promising in vitro models to study the human heart microenvironment. Scientific reports. 2017; 7(1):1–12.

Richards DJ, Li Y, Kerr CM, Yao J, Beeson GC, Coyle RC, Chen X, Jia J, Damon B, Wilson R, et al. Human cardiac organoids for the modelling of myocardial infarction and drug cardiotoxicity. Nature Biomedical Engineering. 2020; 4(4):446–462.

Rodriguez ML, Graham BT, Pabon LM, Han SJ, Murry CE, Sniadecki NJ. Measuring the contractile forces of human induced pluripotent stem cell-derived cardiomyocytes with arrays of microposts. Journal of biomechanical engineering. 2014; 136(5):051005.

Ronaldson-Bouchard K, Ma SP, Yeager K, Chen T, Song L, Sirabella D, Morikawa K, Teles D, Yazawa M, Vunjak-Novakovic G. Advanced maturation of human cardiac tissue grown from pluripotent stem cells. Nature. 2018; 556(7700):239–243.

Saini H, Navaei A, Van Putten A, Nikkhah M. 3D cardiac microtissues encapsulated with the co-culture of cardiomyocytes and cardiac fibroblasts. Advanced healthcare materials. 2015; 4(13):1961–1971.

Schaaf S, Shibamiya A, Mewe M, Eder A, Stör A, Hirt MN, Rau T, Zimmermann WH, Conradi L, Eschenhagen T, et al. Human engineered heart tissue as a versatile tool in basic research and preclinical toxicology. PloS one. 2011; 6(10):e26397.

Seguret M, Vermersch E, Jouve C, Hulot JS. Cardiac Organoids to Model and Heal Heart Failure and Cardiomyopathies. Biomedicines. 2021; 9(5):563.

Shadrin IY, Allen BW, Qian Y, Jackman CP, Carlson AL, Juhas ME, Bursac N. Cardiopatch platform enables maturation and scale-up of human pluripotent stem cell-derived engineered heart tissues. Nature communications. 2017; 8(1):1–15.

Sharma A, Li G, Rajarajan K, Hamaguchi R, Burridge PW, Wu SM. Derivation of highly purified cardiomyocytes from human induced pluripotent stem cells using small molecule-modulated differentiation and subsequent glucose starvation. JoVE (Journal of Visualized Experiments). 2015; (97):e52628.

Stillitano F, Turnbull IC, Karakikes I, Nonnenmacher M, Backeris P, Hulot JS, Kranias EG, Hajjar RJ, Costa KD. Genomic correction of familial cardiomyopathy in human engineered cardiac tissues. European heart journal. 2016; 37(43):3282–3284.

552 **Streckfuss-Bömeke K**, Wolf F, Azizian A, Stauske M, Tiburcy M, Wagner S, Hübscher D, Dressel R, Chen S, Jende
553 J, et al. Comparative study of human-induced pluripotent stem cells derived from bone marrow cells, hair
554 keratinocytes, and skin fibroblasts. European heart journal. 2013; 34(33):2618–2629.

555 **Thavandiran N**. Design of Human Pluripotent Stem Cell-derived Cardiac Microtissue-based Platforms for Func-
556 tional Screening. PhD thesis, University of Toronto; 2019.

557 **Tiburcy M**, Hudson JE, Balfanz P, Schlick S, Meyer T, Chang Liao ML, Levent E, Raad F, Zeidler S, Wingender E,
558 et al. Defined engineered human myocardium with advanced maturation for applications in heart failure
559 modeling and repair. Circulation. 2017; 135(19):1832–1847.

560 **Turnbull IC**, Karakikes I, Serrao GW, Backeris P, Lee JJ, Xie C, Senyei G, Gordon RE, Li RA, Akar FG, et al. Advancing
561 functional engineered cardiac tissues toward a preclinical model of human myocardium. The FASEB Journal.
562 2014; 28(2):644–654.

563 **van der Velden J**, Asselbergs FW, Bakkers J, Batkai S, Bertrand L, Bezzina CR, Bot I, Brundel BJ, Carrier L,
564 Chamuleau S, et al. Animal models and animal-free innovations for cardiovascular research: current sta-
565 tus and routes to be explored. Consensus document of the ESC working group on myocardial function and
566 the ESC Working Group on Cellular Biology of the Heart. Cardiovascular research. 2022; 118(15):3016–3051.

567 **Williams K**, Liang T, Massé S, Khan S, Hatkar R, Keller G, Nanthakumar K, Nunes SS. A 3-D human model of
568 complex cardiac arrhythmias. Acta Biomaterialia. 2021; 132:149–161.

569 **Zhao Y**, Rafatian N, Feric NT, Cox BJ, Aschar-Sobbi R, Wang EY, Aggarwal P, Zhang B, Conant G, Ronaldson-
570 Bouchard K, et al. A platform for generation of chamber-specific cardiac tissues and disease modeling. Cell.
571 2019; 176(4):913–927.

572 **Zhuang RZ**, Lock R, Liu B, Vunjak-Novakovic G. Opportunities and challenges in cardiac tissue engineering from
573 an analysis of two decades of advances. Nature Biomedical Engineering. 2022; 6(4):327–338.

A.

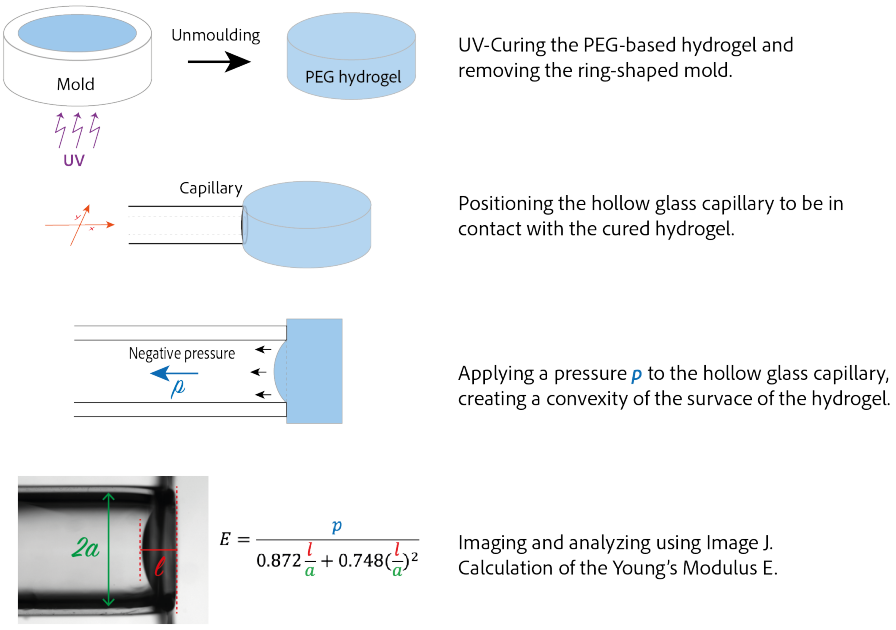

B.

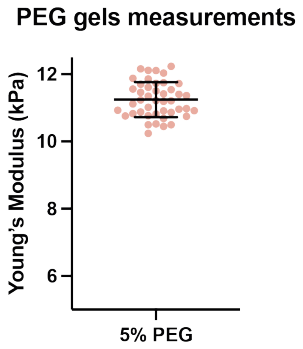

Figure 1—figure supplement 1. A. Procedure to measure the Young's Modulus of a PEG-gel disk by pipette aspiration. **B.** Young's modulus of 5% PEG gels (n=44).

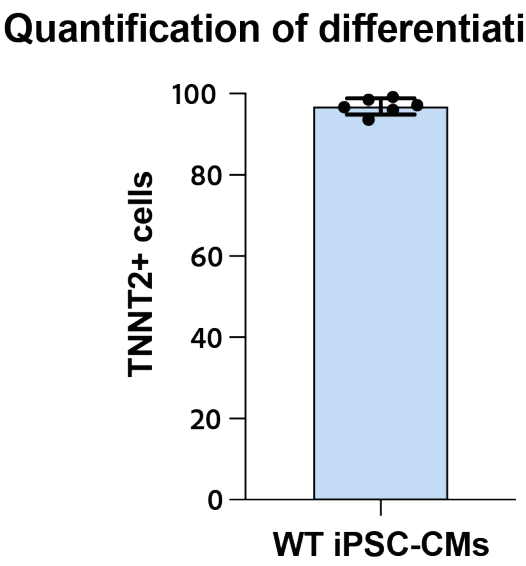

Figure 1—figure supplement 2. Percentage of positive cells for Troponin T2 (TNNT2) determined by flow cytometry in the 6 different differentiations of wild-type (WT) iPSCs, used for these experiments.

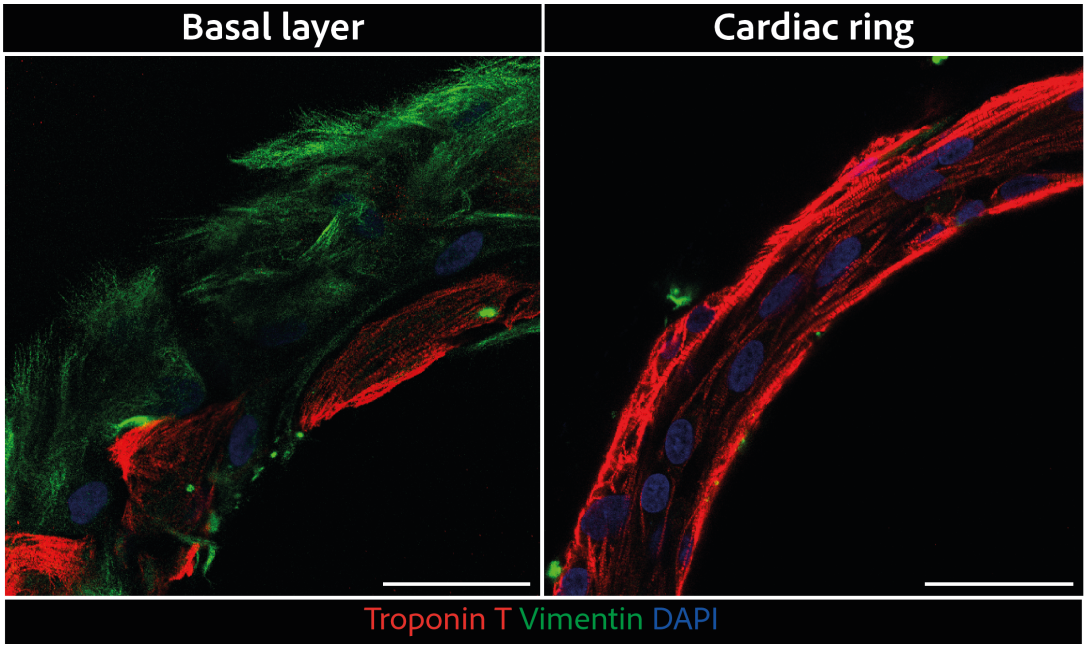

Figure 2—figure supplement 1. Larger scale confocal pictures of immunostained tissues at different heights basal layer(left) and cardiac ring (right) at 40X magnification: vimentin is stained in green, troponin in red, and DAPI in blue. Scale bars: 50 µm.

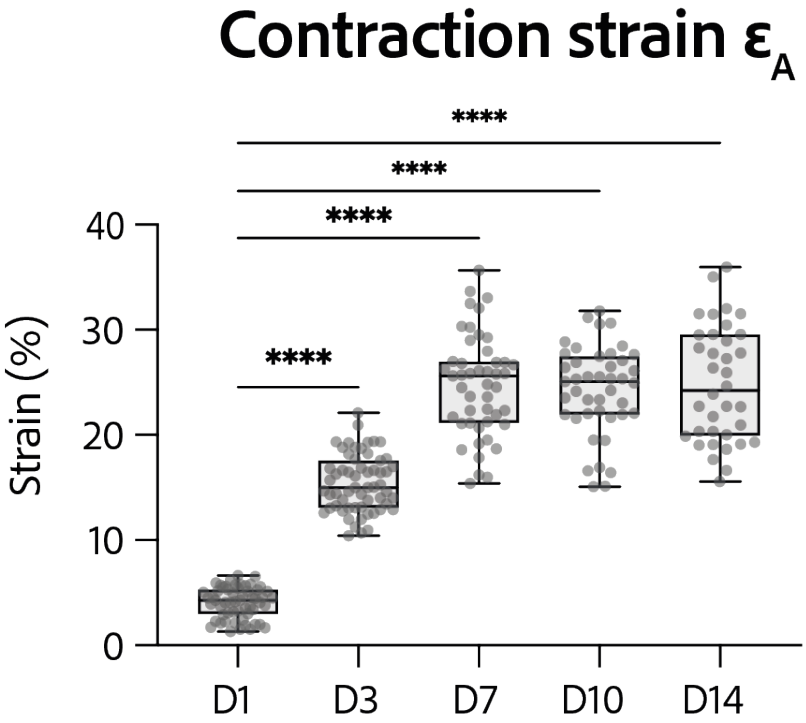

Figure 3—figure supplement 1. Evolution of contraction strain ϵ_A through time after seeding at days 1, 3, 7, 10 and 14. Contraction strain changes through time are significant (p<0.0001 - ANOVA for repeated measures - D1: n=57, D3: n=59 D7: n=47, D10: n=43, D14: n=36 tissues, from 3 differentiations). Contraction strain for each concentration is compared to contraction strain at day 1 (****: p<0.0001).

A.

No fibroblast

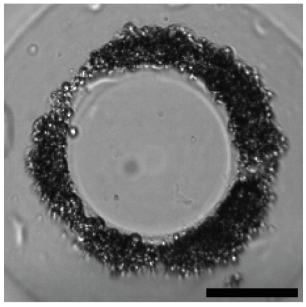

3:1 hiPSC-CMs:fibroblasts

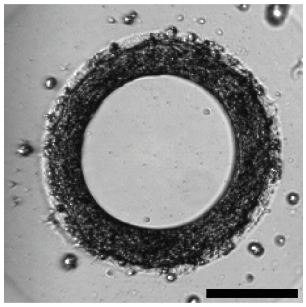

B.

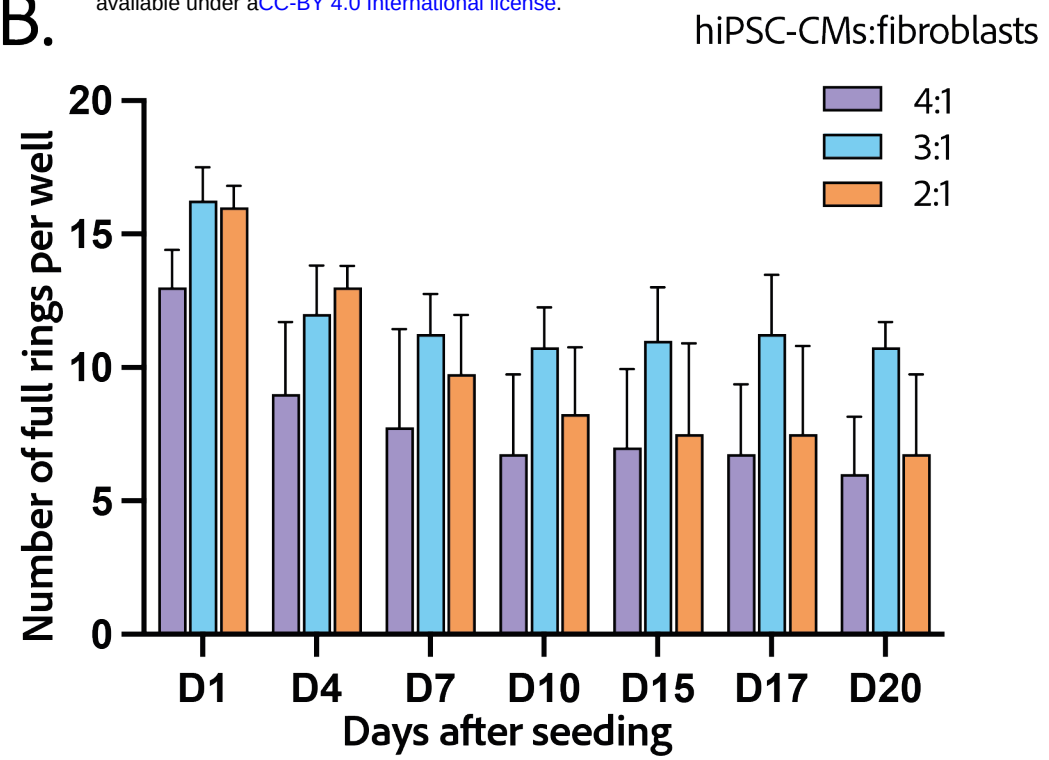

C.

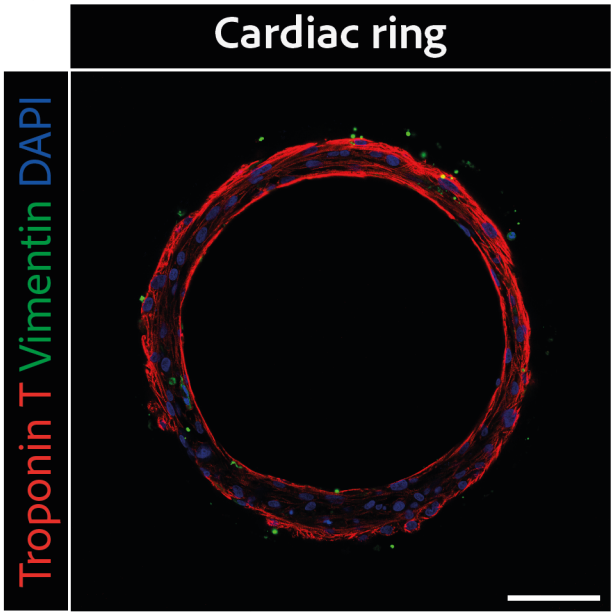

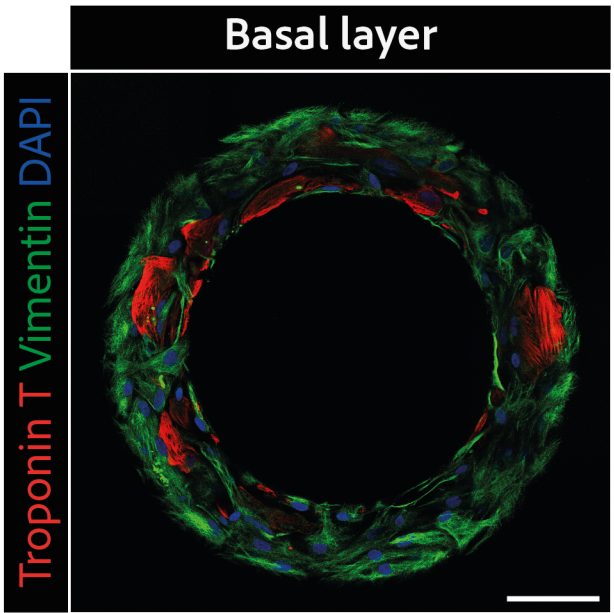

D.

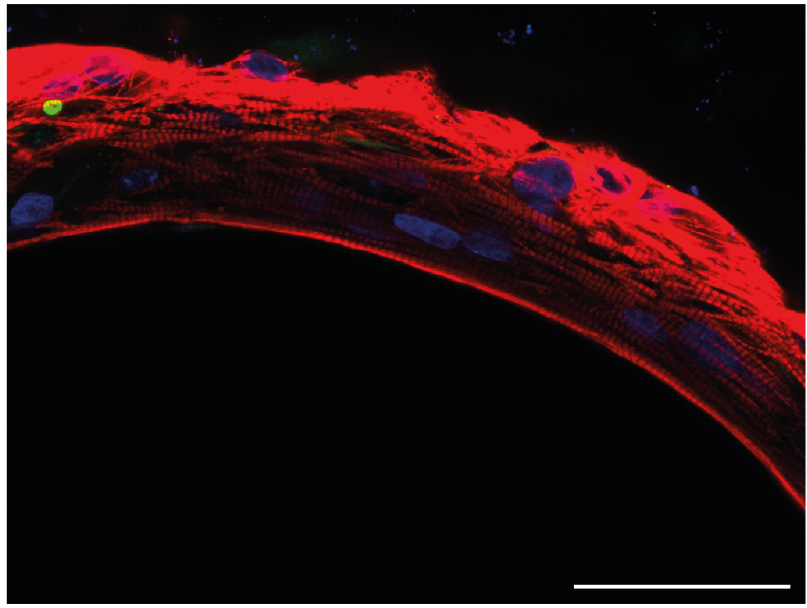

E.

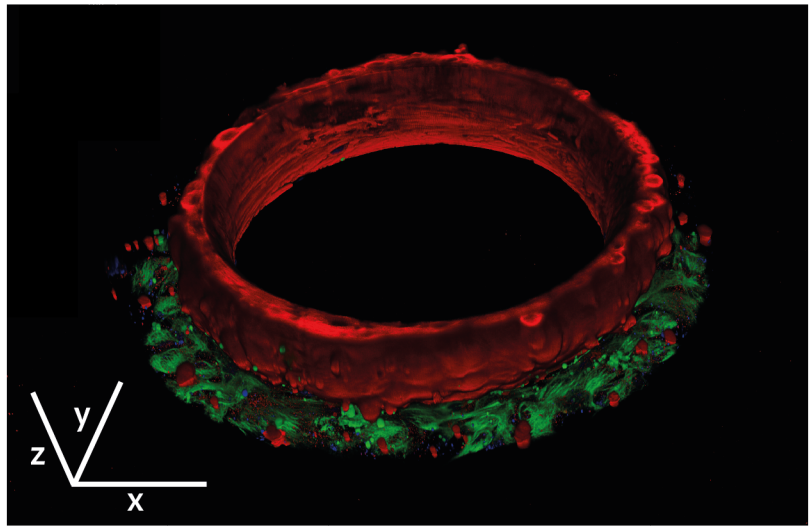

A.

Monitoring of the area of the central pillar

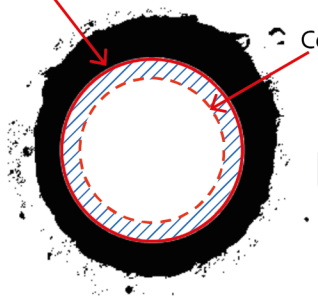

Strain in time $\varepsilon_A(t)$

$$\varepsilon_A(t) = \frac{Max(Area) - Area(t)}{Max(Area)}$$

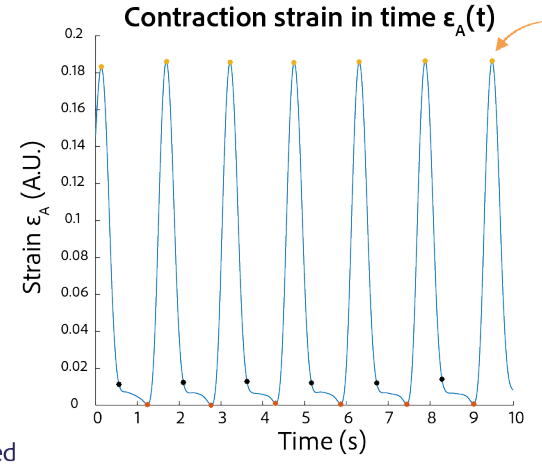

$$\frac{d(\varepsilon_A(t))}{dt}$$

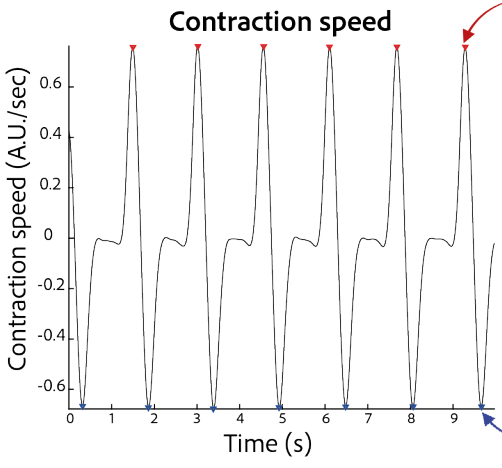

B.

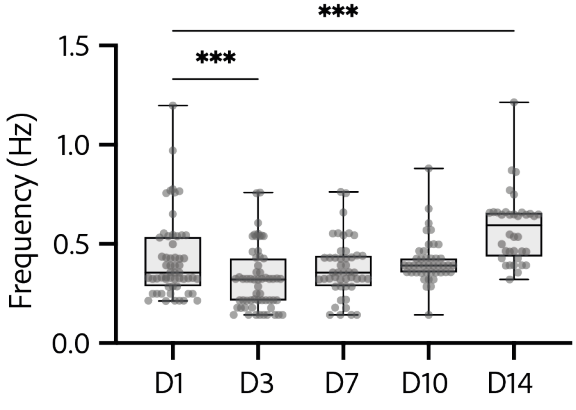

C.

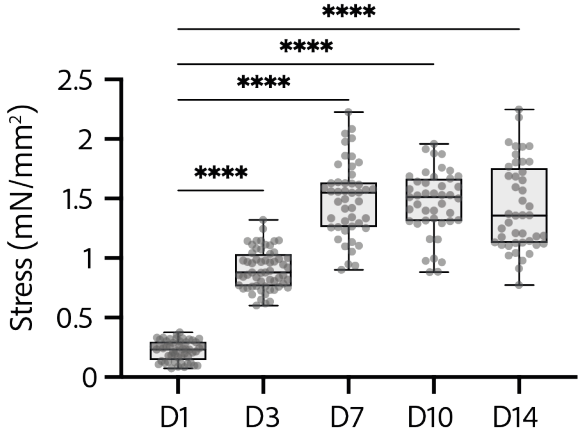

D.

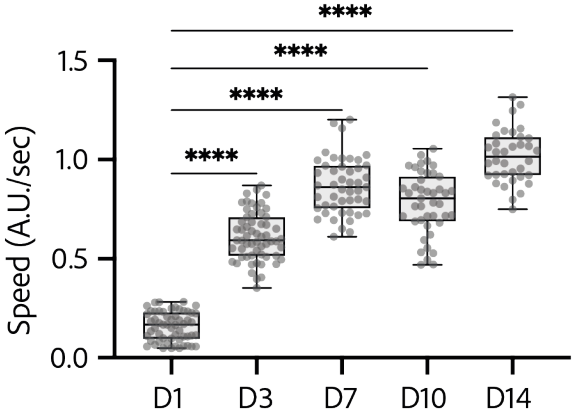

E.

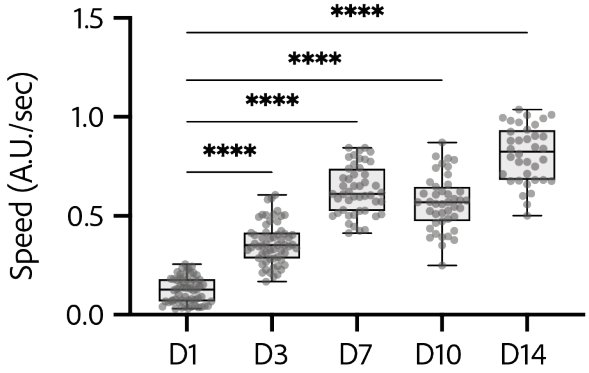

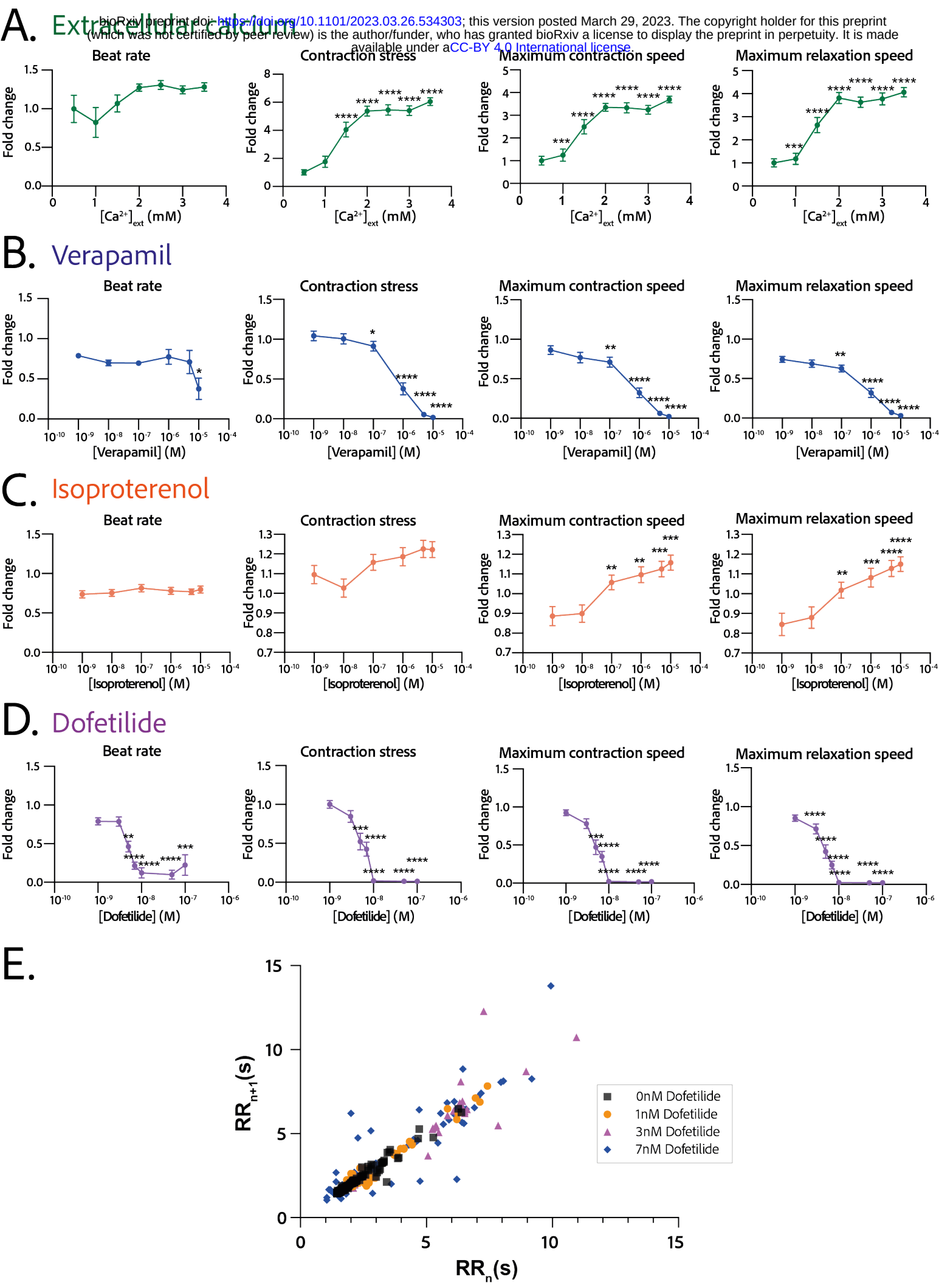

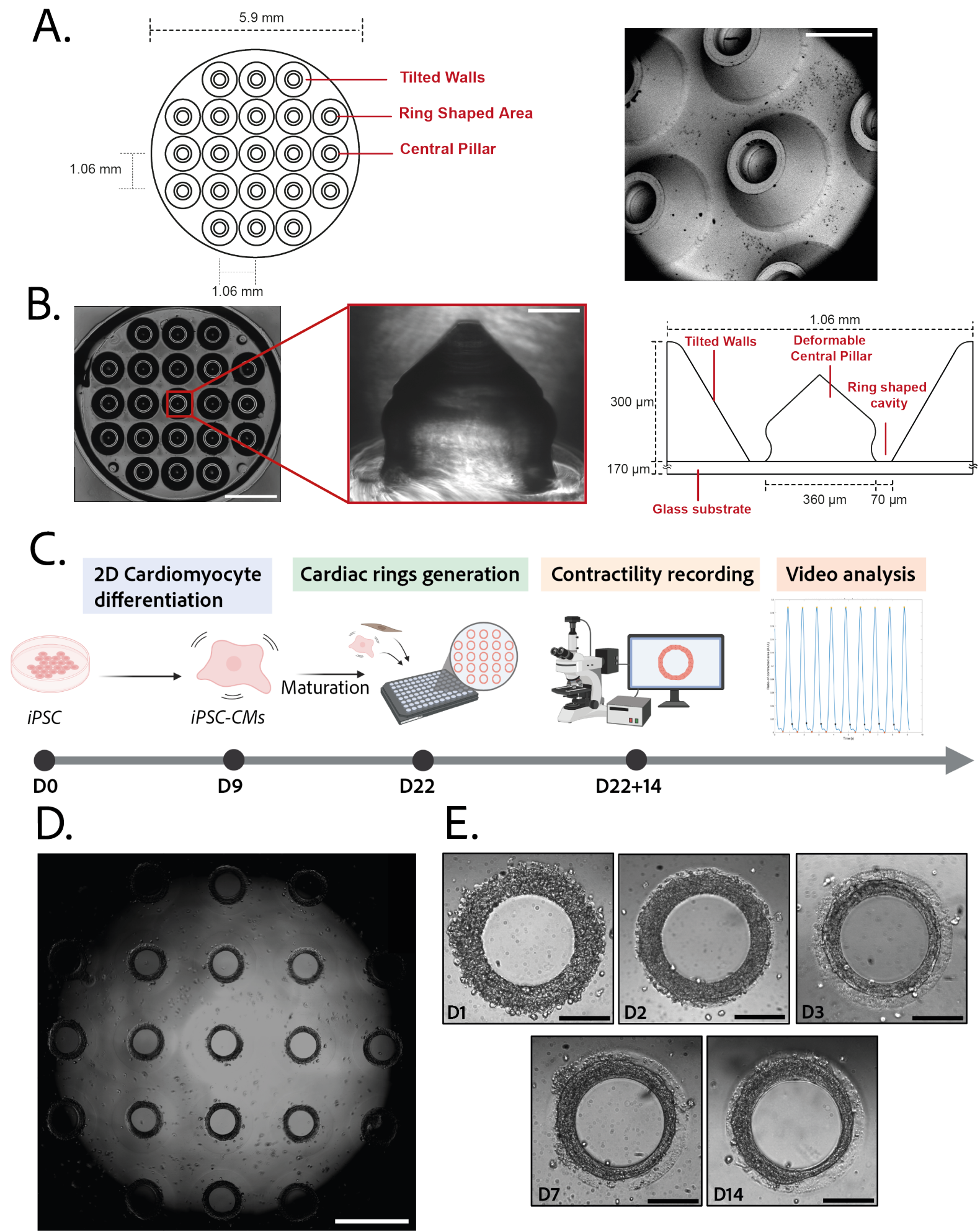
A.
5.9 mm
Tilted Walls
Ring Shaped Area
Central Pillar
1.06 mm
1.06 mm
B.
1.06 mm
Tilted Walls
Deformable Central Pillar
Ring shaped cavity
300 µm
170 µm
Glass substrate
360 µm
70 µm
C.
2D Cardiomyocyte differentiation
Cardiac rings generation
Contractility recording
Video analysis
iPSC
iPSC-CMs
Maturation
D0
D9
D22
D22+14
D.
E.
D1
D2
D3
D7
D14

A.

1

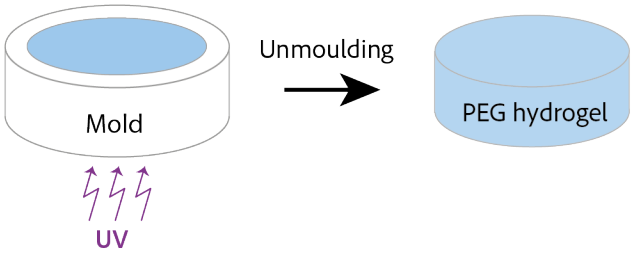

UV-Curing the PEG-based hydrogel and removing the ring-shaped mold.

2

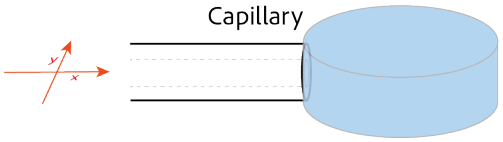

Positioning the hollow glass capillary to be in contact with the cured hydrogel.

3

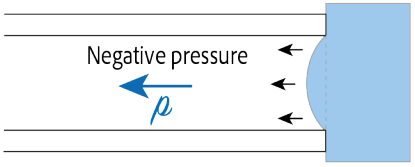

Applying a pressure *p* to the hollow glass capillary, creating a convexity of the survace of the hydrogel.

4

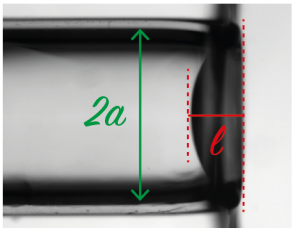

$$E = \frac{p}{0.872\frac{l}{a} + 0.748(\frac{l}{a})^2}$$

Imaging and analyzing using Image J.
Calculation of the Young's Modulus E.

B.